JOURNAL OF GEOPHYSICAL RESEARCH, VOL. 111, A08304, doi:10.1029/2006JA011598, 2006

Click Here for Full Article

Solar activity variations of the ionospheric peak electron density

Libo Liu,[1] Weixing Wan,[1] Baiqi Ning,[1] O. M. Pirog,[2] and V. I. Kurkin[2]

Received 1 January 2006; revised 26 April 2006; accepted 24 May 2006; published 31 August 2006.

[1] The daily averaged Solar EUV Monitor (SEM)/Solar Heliospheric Observatory (SOHO) EUV measurements, solar proxies, and foF2 data at 20 ionosonde stations in the east Asia/Australia sector are collected to investigate the solar activity dependences of the ionospheric peak electron density (NmF2). The intensities of solar EUV from the SEM/SOHO measurements from 1996 to 2005 show a nonlinear relationship with F107, and the SEM/SOHO EUV can be better represented by a solar activity factor P = (F107 + F107A)/2. Seasonal and latitudinal dependences are found in the solar activity variation of NmF2 in the east Asia/Australian sector. The slope of NmF2 with P in the linear segment further shows similar annual variations as the background electron densities at moderate solar activity. Observations show a nonlinear dependence of NmF2 on solar EUV (the saturation effect of NmF2 for high solar EUV). On the basis of a simple model of photochemistry, taking the neutral atmospheric consequences into account, calculations at fixed height simulate the saturation effect of NmF2, but the observed change rate of NmF2 with P is inadequately reproduced. Calculations taking into account the influence of dynamics (via a simple model of the solar EUV dependence of the ionospheric height) tend to reproduce the observed change rate of NmF2. Results indicate that besides solar EUV changes, the influence of dynamics and the atmospheric consequences should substantially contribute to the solar activity variations of NmF2.

Citation: Liu, L., W. Wan, B. Ning, O. M. Pirog, and V. I. Kurkin (2006), Solar activity variations of the ionospheric peak electron density, *J. Geophys. Res.*, *111*, A08304, doi:10.1029/2006JA011598.

1. Introduction

[2] The ionosphere is subjected to diurnal, seasonal, solar cycle, and spatial variations [e.g., *Rishbeth and Garriott*, 1969; *Ivanov-Kholodny and Mikhailov*, 1986; *Brekke*, 1997; *Kawamura et al.*, 2002; *Yu et al.*, 2004]. It is well established that the formation of the ionosphere is primarily due to the ionization of the upper atmosphere by solar X-ray and extreme ultraviolet (EUV) radiations of wavelengths less than 1026 Å [*Adler et al.*, 1997], which are known to have different period variations, especially the well-known solar cycle variations [*Kane*, 1992, 2003; *Lean et al.*, 2001; *Tobiska et al.*, 2000]. Observations indicate that parameters of the Earth's ionosphere, such as the critical frequency (foF2), the peak electron density of the *F* region (NmF2), and the total electron content (TEC), are strongly controlled by solar activity in a rather complicated way [e.g., *Adler et al.*, 1997; *Balan et al.*, 1994, 1996; *Bilitza*, 2000; *Huang and Cheng*, 1995; *Kane*, 1992, 2003; *Kouris et al.*, 1998; *Kuznetsov et al.*, 1998; *Lei et al.*, 2005; *Liu et al.*, 2003, 2004a, 2004b, 2006; *Mikhailov and Mikhailov*, 1995a, 1995b; *Pancheva and Mukhtarov*, 1998; *Rao and Rao*, 1969; *Richards*, 2001; *Richards et al.*, 1994b; *Rishbeth*, 1993; *Sethi et al.*, 2002; *Sojka et al.*, 2006; *Su et al.*, 1999].

[3] Solar proxies have been used to represent solar emissions in the absence of continued long-term records of solar EUV fluxes, since the variations of solar EUV radiations are the primary cause for changes in the ionosphere. Sunspot number and solar 10.7 cm radio noise, F107, are commonly used as proxies for solar activity [e.g., *Bilitza*, 2000]. By examining the relationship between a monthly median foF2 (or NmF2) and a smoothed sunspot number (or F107), studies show that foF2 (or NmF2) linearly increases, for low values of sunspot numbers or F107. However, at high values of the sunspot numbers or F107, median foF2 (or NmF2) tends to saturate. This saturation effect is also found in TEC [e.g., *Balan et al.*, 1994]. It is still controversial whether the ionospheric saturation effect is a true manifestation of solar activity effect, and what cause the saturation effect. *Balan et al.* [1994] proposed that the ionospheric saturation effect is due to the nonlinearity of solar EUV with F107. *Balan et al.* [1994, 1996] stated that the ionospheric saturation effect is absent in TEC or NmF2 against solar EUV. Recently, *Liu et al.* [2003] found that the foF2 saturation effect still appears for the EUV radiations and postulated that the daily ionospheric equatorial fountain and prereversal enhancement are important for the saturation features. The problems with modeling the solar EUV have been discussed by *Richards et al.* [1994a] and *Mikhailov and Schlegel* [2000]. Moreover, there is weak or no correlation found between daily noon-

[1] Institute of Geology and Geophysics, Chinese Academy of Sciences, Beijing, China.
[2] Institute of Solar-Terrestrial Physics, Russian Academy of Sciences, Irkutsk, Russia.

Copyright 2006 by the American Geophysical Union.
0148-0227/06/2006JA011598$09.00

Table 1. List of the Ionosonde Stations From Which Ionospheric Data Were Analyzed

Station	Geographic Latitude	Geographic Longitude	Geomagnetic Latitude	Dip	Years Analyzed
Yakutsk	62.0	129.6	51.5	75.7	1957–1998 and 2000–2001
Magadan	60.0	151.0	51.1	71.3	1968–1990 and 1995
Irkutsk	52.5	104.0	41.5	71.1	1957–1997, 1999, and 2003–2004
Khabarovsk	48.5	135.1	38.4	63.6	1959–1983 and 1986–1990
Wakkanai	45.4	141.7	35.8	59.5	1948–1988, 1992–1993, and 1996–2005
Akita	39.7	140.1	29.9	53.5	1957–1989
Kokubunji	35.7	139.5	25.9	48.8	1957–2005
Yamagawa	31.2	130.6	20.8	44.0	1957–1988 and 1996–2005
Wuhan	30.5	114.4	19.5	45.0	1948–1993 and 1995–2004
Okinawa	26.3	127.8	15.8	36.6	1957–1989, 1992–1993, and 1996–2005
Taipei	25.0	121.5	14.2	35.1	1959–1989
Manila	14.6	121.1	3.8	14.3	1964–1989
Vanimo	−2.7	141.3	−12.0	−22.7	1964–2004
Darwin	−12.5	130.9	−23.2	−41.1	1982–2004
Townsville	−19.3	146.7	−28.4	−49.2	1951–2004
Norfolk Is.	−29.0	168.0	−34.8	−56.8	1964–2005
Brisbane	−27.5	152.9	−35.7	−58.1	1950–1986 and 2001–2005
Mundaring	−32.0	116.3	−43.5	−66.9	1959–2004
Canberra	−35.3	149.0	−44.0	−66.5	1950–2004
Hobart	−42.9	147.2	−51.6	−73.0	1950–2005

time NmF2 and F107 during a relatively short period (although F107 has large changes) [*Rishbeth*, 1993; *Richards et al.*, 1994b; *Richards*, 2001]. Finally, statistical analyses show that foF2 also depends on historical solar activities [*Pancheva and Mukhtarov*, 1998; *Liu et al.*, 2004a]. Even for the same solar level, foF2 may have different values during different phases of a solar cycle, namely the ''hysteresis'' effect [*Kane*, 1992; *Mikhailov and Mikhailov*, 1995a; *Rao and Rao*, 1969; *Triskova and Chum*, 1996]. On the other hand, the solar EUV changes as such itself were inadequate for causing observed changes in NmF2 [*Kane*, 2003]. However, the contributions from various factors to the solar activity effects of NmF2 are not evaluated yet.

[4] Considerable progress has been made in understanding the solar cycle variations of monthly median NmF2 or foF2 [e.g., *Kane*, 1992; *Sethi et al.*, 2002; *Liu et al.*, 2003, 2004a]. However, there are limited analyses applied to the daily values [*Kouris et al.*, 1998]. The day-to-day changes of the ionosphere are not necessarily due to the solar variability [*Forbes et al.*, 2000]. It is expected that the significant day-to-day changes must inevitably degrade the correlations [*Kouris et al.*, 1998; *Rishbeth*, 1993]. This situation calls for examining to what extent the daily values depend on daily solar activity. Moreover, we know that shorter wavelength radiation generally originates higher in the solar atmospheres [*Brekke*, 1997; *Floyd et al.*, 2005] and the emission mechanisms are different in detail [*Lean et al.*, 2001]. Neither F107 nor the sunspot number is ideal for representing the solar EUV emission variability [*Ivanov-Kholodny and Mikhailov*, 1986; *Lean et al.*, 2001]. Therefore long-term solar EUV observations are required urgently for better understanding the solar activity variations of the ionosphere.

[5] This paper reports an analysis based on a longer series of daily solar EUV data and NmF2 data at 20 ionosonde stations in the east Asia/Australian sector. Since 1996, solar EUV fluxes in 26–34 nm and 0.1–50 nm wavelength ranges were continuously monitored by the Solar EUV Monitor (SEM) spectrometer aboard the Solar Heliospheric Observatory (SOHO) [*Judge et al.*, 1998]. The SEM/SOHO EUV observations provide a good opportunity to study the solar activity variability in the ionosphere.

[6] The objective of this work is threefold: to access the saturation effect of NmF2 with the observed SEM/SOHO EUV data; to quantify the solar activity dependence of NmF2 in the east Asia/Australian sector; and to evaluate the dynamic effects and the atmospheric consequences of the solar activity effects of NmF2.

2. Data

[7] Since the International Geophysical Year, ionospheric data have been greatly and rapidly accumulated. However, there are gaps in the ionospheric data archived in one World Data Centers (WDC). We bridge the gaps in the data series of foF2 which is provided from WDCs in the United States, Japan, and Australia. Data at Wuhan are collected from Wuhan Ionospheric Observatory of the Institute of Geology and Geophysics of the Chinese Academy of Sciences, and data at Irkutsk and Yakutsk are collected from the Institute of Solar-Terrestrial Physics of Russia. The foF2 collected for this analysis spans more than 50 years at some stations with the above augmentations.

[8] NmF2 used for this study is evaluated from foF2 ($NmF2 = 1.24 \times 10^4\ (foF2)^2$, NmF2 in unit of electron/cm^3, foF2 in MHz), the critical frequency of the F2 layer, which is routinely recorded at 20 ionosonde stations in the east Asia/Australian sector, spanning from 42.9°S to 62.0°N geographical latitudes and from −51.6 to 51.5 geomagnetic latitudes. The names and the locations of these 20 stations are listed in Table 1. In present work, our emphasis is focused on the seasonal and latitudinal features of the solar activity dependence of daytime NmF2 as described afterward. As the calculations are supposed to deal with a stationary F2 layer, only data around local noontime are selected. Note that the NmF2 data with the geomagnetic activity index Ap > 20 nT are excluded during the previous

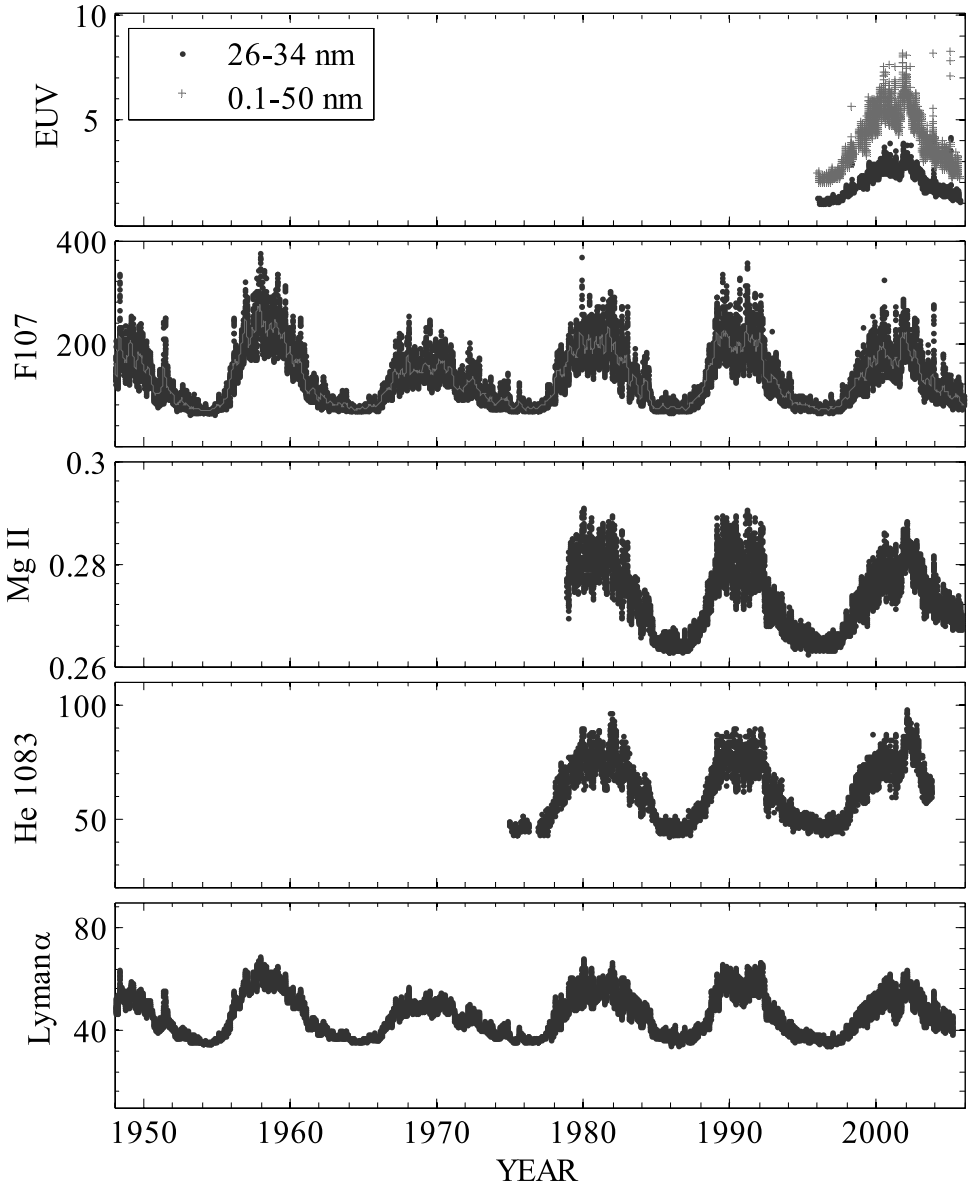

Figure 1. Time series of solar indices, F107, solar Mg II index, He 1083 (the equivalent width of the helium 1083 nm solar absorption line), Lyman α, during 1948–2005 and SOHO/SEM EUV fluxes at 0.1–50 and 26–34 nm wavelength bands during 1996–2005, respectively. F107 and its 81 days average, F107A, in unit of 10^{-22} W m^{-2} Hz^{-1}, He 1083 in mÅ, Lyman α in 10^{10} photons cm^{-2} s^{-1}, and SOHO/SEM EUV fluxes in unit of 10^{10} photons cm^{-2} s^{-1}.

48 hours to minimize geomagnetic effects. The remaining data are grouped into bins at each station according to month.

[9] The daily values of the SEM/SOHO EUV fluxes are available from 1996 at http://www.usc.edu/dept/space_science/semdatafolder/long/. Four solar activity indices are included for this analysis. The daily NOAA Mg II index is a composite solar proxy from the Mg II core-to-wing ratio [*Viereck and Puga*, 1999; *Viereck et al.*, 2004], which was prepared by the U.S. Dept. of Commerce, NOAA, Space Environment Center. Mg II index spans from 1978 to 2005. Daily Lyman α (121.6 nm) irradiance [*Woods and Rottman*, 1997] data are downloaded from the National Solar Observatory/Kitt Peak website. He 1083 index [*Harvey*, 1984] is the full disk-averaged value of the equivalent width of the He 1083 nm infrared absorption line, which formed entirely in the chromosphere. The F107 and Ap indices are downloaded from SPIDR. The SEM/SOHO EUV fluxes and these solar activity proxies used in the analysis are plotted in Figure 1.

[10] Mass plots of these solar data sets against F107 and (F107 + F107A)/2 are illustrated in Figure 2, and the corresponding linear correlation coefficients are listed in Table 2. Here F107A is the 81-day average of F107. The linear correlation coefficient $r(X, Y)$ is calculated using

$$r(X,Y) = \frac{\mathrm{Cov}(X,Y)}{\sqrt{\mathrm{Cov}(X,X)\mathrm{Cov}(Y,Y)}}, \qquad (1)$$

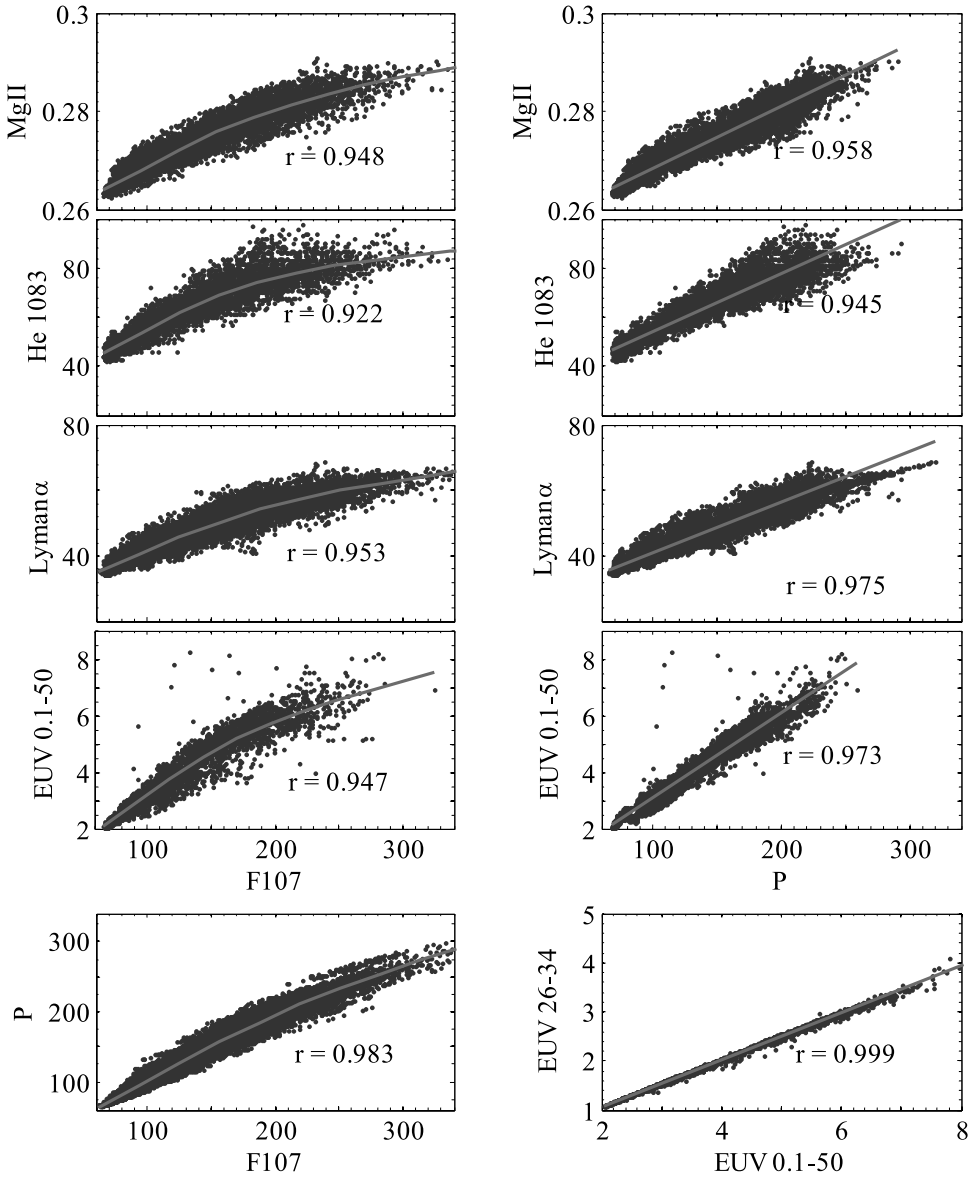

Figure 2. Correlations among the various solar data sets in Figure 1. Solar activity factor P = (F107 + F107A)/2. The related linear correlation coefficients, r, are also labeled. F107 and P in unit of 10^{-22} W m^{-2} Hz^{-1}, He 1083 in mÅ, Lyman α in 10^{10} photons cm^{-2} s^{-1}, and SOHO/SEM EUV fluxes in unit of 10^{10} photons cm^{-2} s^{-1}.

where the covariance between data set X and Y, $\mathrm{Cov}(X,Y) = E\{[X - E(X)]\,[Y - E(Y)]\}$, and $E(X)$ is the mathematical expectation of X.

3. Results and Discussions

3.1. Solar EUV and Solar Proxies

[11] Figure 2 (bottom right) shows a strongly linear correlation (a correlation exceeding +0.99) between the two EUV bands (0.1–50 nm and 26–34 nm) obtained from the SEM/SOHO from 1996 to 2005. The highly intercorrelation feature is also reported previously [*Bilitza*, 2000; *Kane*, 2003]. Thus we will only take the 0.1–50 nm EUV flux data to present the dependence of NmF2 on solar EUV.

[12] As shown in Figure 2, the intensities of SEM/SOHO EUV are apparently nonlinear with the current day F107,

Table 2. Correlation Coefficients Among the Various Solar Data Sets in Figure 1[a]

	F107	P	Mg II	He 1083	Lyman α	EUV 0.1–50	EUV 26–34
F107	1	**0.983**	**0.947**	**0.921**	**0.952**	**0.946**	**0.937**
P	(21154)	1	**0.957**	**0.944**	**0.974**	**0.972**	**0.967**
Mg II	(8550)	(8550)	1	**0.971**	**0.970**	**0.942**	**0.941**
He 1083	(6259)	(6259)	(4930)	1	**0.954**	**0.950**	**0.952**
Lyman α	(20877)	(20877)	(8340)	(6259)	1	**0.953**	**0.953**
EUV 0.1–50	(3384)	(3384)	(3101)	(1865)	(3215)	1	**0.999**
EUV 26–34	(3330)	(3330)	(3050)	(1828)	(3161)	(3330)	1

[a]Bold values are the correlation coefficients in each regression. Values in parentheses are the number of pairs of points in each regression.

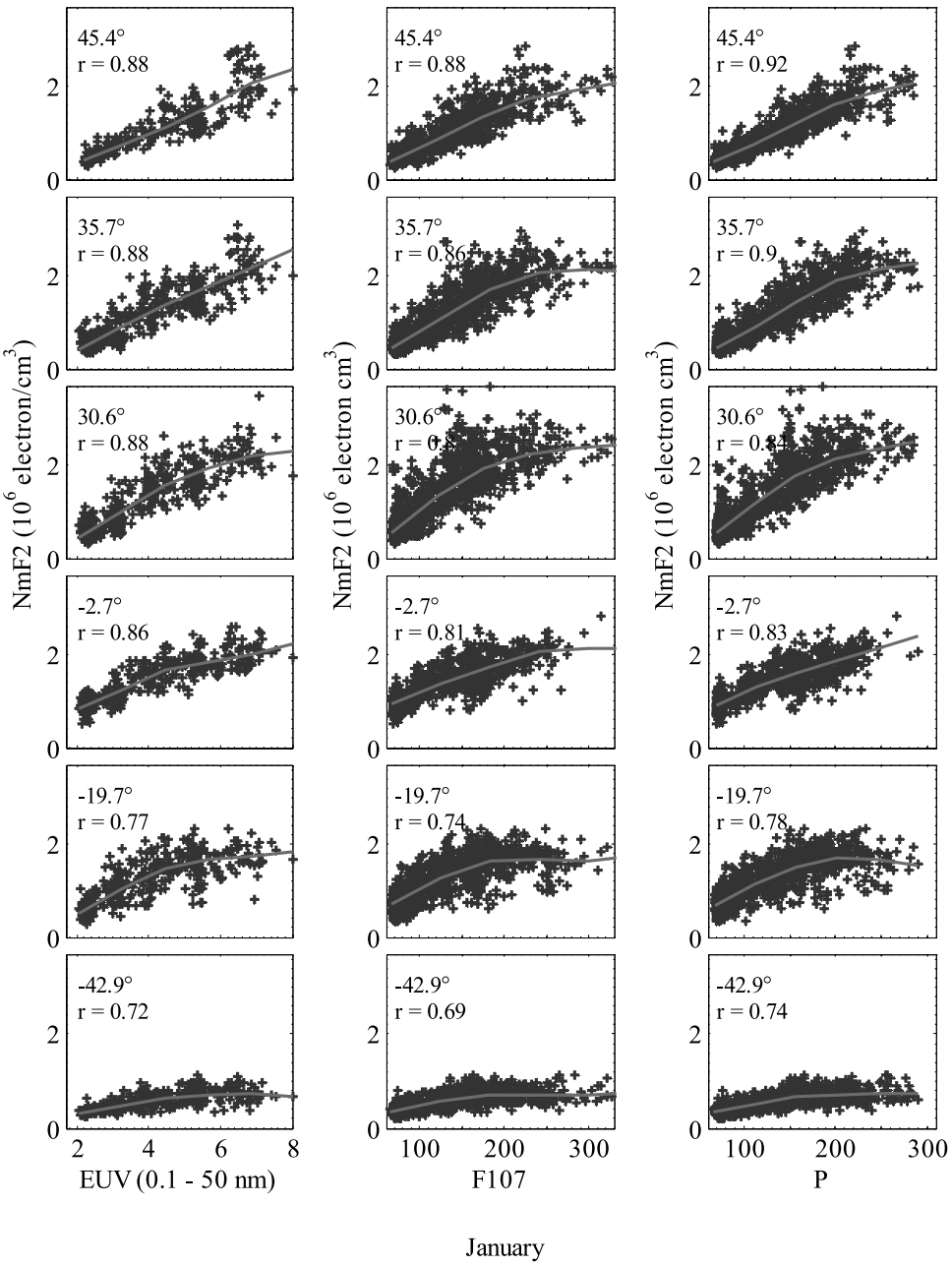

Figure 3. Solar activity dependences of daily NmF2 on EUV flux, F107, and P at six sample stations in January. F107 and P in unit of 10^{-22} W m^{-2} Hz^{-1}, SOHO/SEM EUV fluxes in 10^{10} photons cm^{-2} s^{-1}, and NmF2 in 10^6 electron cm^{-3}. See the text in detail.

although their correlation coefficient is high ($r \sim 0.94$). The same feature is found for solar proxies shown in Figure 1. The increase of SEM/SOHO EUV with F107 is much steeper at low and moderate F107 values than at high ones. Inspection of Table 2 confirms that in a gross way, different solar proxies show a similar solar cycle variation [*Bilitza*, 2000; *Floyd et al.*, 2005; *Ivanov-Kholodny and Mikhailov*, 1986; *Viereck et al.*, 2004] and very high correlation is evident among those solar indices. However, as illustrated in Figure 2, on a finer scale, there are considerable differences, which are consistent with previous works [*Balan et al.*, 1994; *Floyd et al.*, 2005; *Lean et al.*, 2001; *Richards et al.*, 1994a]. The differences reflect the temporal and spatial structures between source regions of chromospheric and coronal radiations [*Lean et al.*, 2001].

[13] *Hinteregger et al.* [1981] and *Richards et al.* [1994a] took a solar activity factor P, (F107 + F107A)/2, as the scaling factor of solar activity. As shown in Figure 2 and Table 2, it can be found that the solar activity factor P is more suitable than F107 as a linear indicator of the SEM/SOHO EUV, because the nonlinearity of SEM/SOHO EUV with P evidently diminishes, and the correlation is also slightly higher. Changes of the solar proxies, H Lyman α, He I 1083, and Mg II, are more linear with P than those with F107. Therefore P will be taken as an indicator of solar activity in the following analysis.

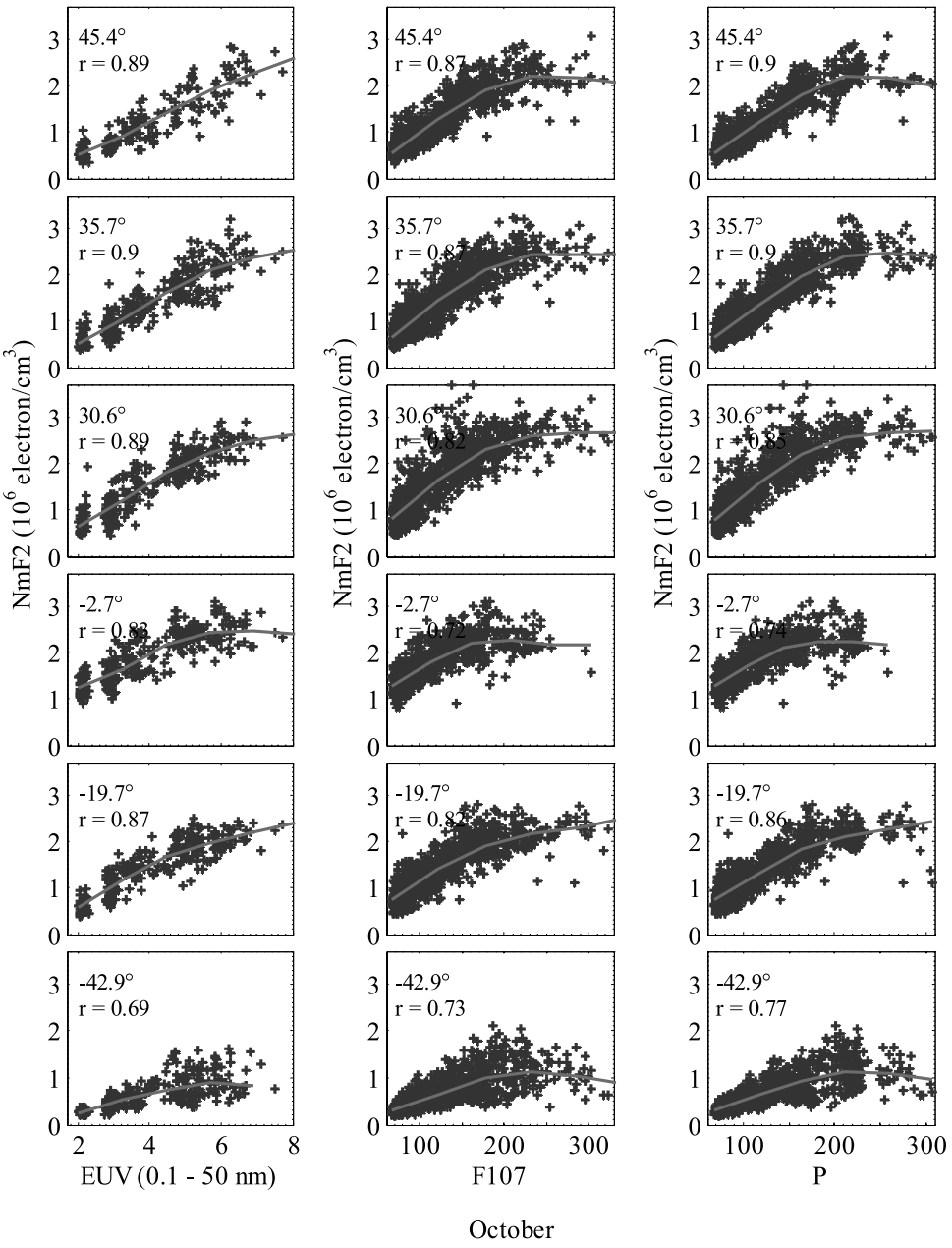

Figure 4. Same as Figure 3 except in October.

3.2. Relationships Between NmF2 and Solar EUV, F107, and P

[14] Mass plots of NmF2 against the SEM/SOHO EUV, F107, and P in January and October at six stations are shown in Figures 3 and 4, respectively. It should be pointed out that data from 1948 to 2005 are shown in Figures 3 and 4 (middle and right), but only data from 1996 to 2005 are shown in Figures 3 and 4 (left); that is, the size of data pairs is much larger for NmF2 with F107 or P in this analysis. In general, the behavior of NmF2 with P is rather similar to that with the observed solar EUV. It is clearly seen that the solar activity variations of daily NmF2 are distinct with latitudinal and seasonal features.

[15] As seen in Figures 3 and 4, the increase of NmF2 with F107 is much steeper at low and moderate F107 values than at high ones. Saturation effects of NmF2 with solar EUV or P are significant at some stations but weak at other stations. This result shows that the saturation effect has latitudinal dependence, and correlation coefficients between NmF2 and solar EUV or P are slightly higher than that with F107. Interesting, the saturation effect exists in the current NmF2 data sets versus not only F107 or P but also solar EUV at stations such as Wuhan (114.4°E, 30.6°N), Vanimo (141.3°E, 2.7°S), Townsville (146.7°E, 19.7°S), and even Hobart (147.2°E, 42.9°S). This is not consistent with that of *Balan et al.* [1994, 1996] in which TEC or NmF2 responds nonlinearly to F107, but linearly to the solar EUV. Thus our result shows an experimental evidence of the saturation effect of NmF2 with the solar EUV and substantiates that the ionospheric saturation effect seems caused not only by

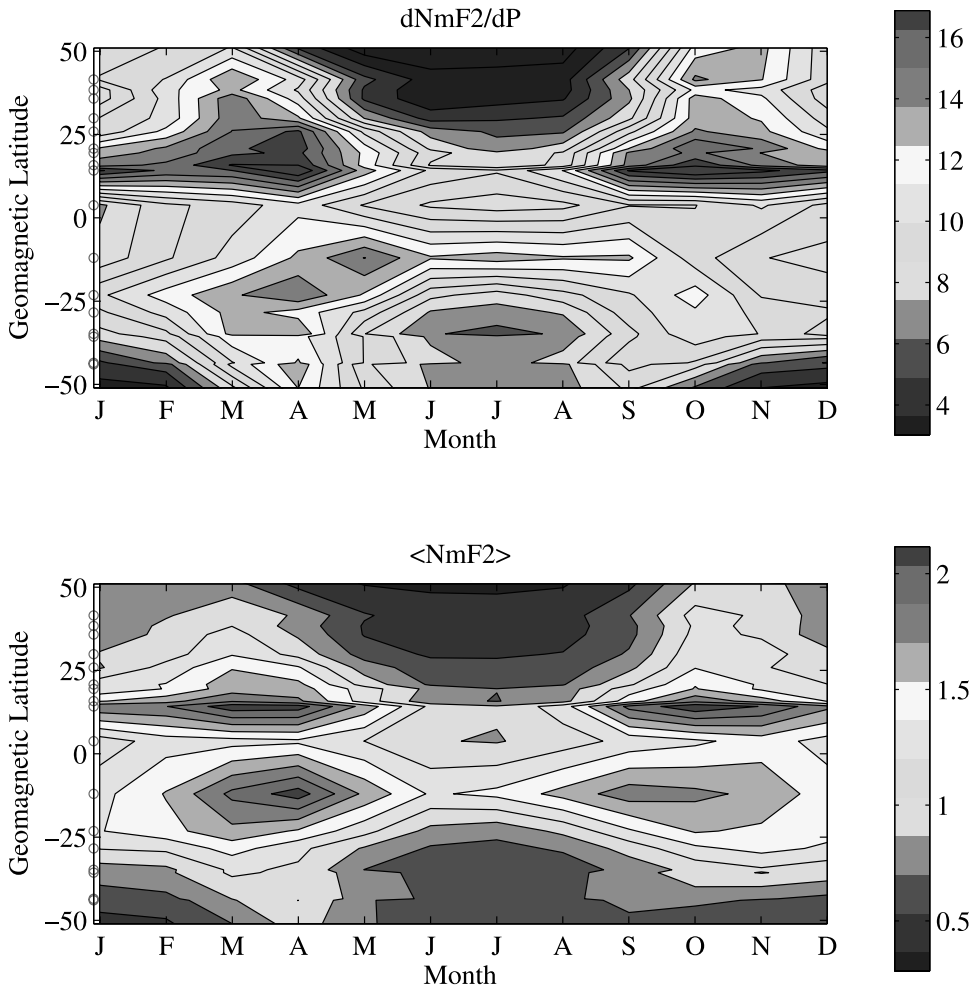

Figure 5. Latitude and season variations of the slope of NmF2 with P, dNmF2/dp, in the linear segment and fitted NmF2 $\langle$NmF2$\rangle$ at P = 120 $\times$ 10^{-22} W m^{-2} Hz^{-1} at stations in the east Asia/Australian sector. $\langle$NmF2$\rangle$ is in 10^6 electron cm^{-3} and dNmF2/dp in units of 10^3 electron cm^{-3} per 10^{-22} W m^{-2} Hz^{-1}.

the manifestation of the solar EUV by F107, but also by other factors, which will be presented in Section 3.4.

3.3. Change Rate of NmF2 With Respect to Solar Activity, dNmF2/dP

[16] As shown in Figures 3 and 4, despite scatter in the data and the saturation effect that occurs at extreme solar activity, a linear relation statistically exists between NmF2 and EUV or P in the lower segment of P (within about 70–170 $\times$ 10^{-22} W m^{-2} Hz^{-1}). The slope dNmF2/dP of this linear segment is a parameter quantifying the solar activity sensitivity of NmF2, which is obtained with a linear regression fitting between daily NmF2 and P for the linear segment:

$$\mathrm{NmF2} = \mathrm{NmF2}_{\mathrm{P}=\mathrm{P}_0} + \frac{\mathrm{dNmF2}}{\mathrm{dP}}(\mathrm{P} - \mathrm{P}_0). \qquad (2)$$

Here $\mathrm{NmF2}_{\mathrm{P}=\mathrm{P}_0}$ is the fitted NmF2 with P of a value P_0, and P_0 (=120, in unit of 10^{-22} W m^{-2} Hz^{-1}) somewhat stands for the median value of P.

[17] Figure 5 displays the seasonal and latitudinal variations of $\mathrm{NmF2}_{\mathrm{P}=120}$ and dNmF2/dP in the east Asia/Australian sector. As can be seen, the noontime $\mathrm{NmF2}_{\mathrm{P}=120}$ is highest at equinoxes; it is higher in winter than in summer. The higher noontime electron density in winter is a manifestation of the well-known winter anomaly, which is mainly explained by the O/N2 effect [*Rishbeth and Setty*, 1961; *Rishbeth et al.*, 2000; *Yu et al.*, 2004]. A pronounced feature in the latitudinal variation of $\mathrm{NmF2}_{\mathrm{P}=120}$ is the equatorial anomaly, which is significant in equinoxes and the northern hemisphere winter and weak or absent in months from June to August. With increasing solar activity, NmF2 increases at a rate of 3000–15,000 electrons cm^{-3} per 10^{-22} W m^{-2} Hz^{-1}. On the other hand, the slope dNmF2/dP also changes with latitude and season. As seen in Figure 5, the highest dNmF2/dP is found near the crests of the equatorial anomaly similar to the background electron densities $\mathrm{NmF2}_{\mathrm{P}=120}$. With season, dNmF2/dP tends to be least in summer, greatest at equinoxes, and intermediate in winter at most stations, except at Vanimo (2.7°S, 141.3°E). At Vanimo, the slope presents an annual variation, higher at the months from May to September and lower in the winter months. Note that our results are consistent with *Huang and Cheng* [1995] and *Rastogi and Sharma* [1971] for TEC.

[18] Our further analysis for NmF2 at midlatitude stations in the northern hemisphere, such as Dourbes (50.1°N, 4.6°E), Kiev (50.5°N, 30.5°E), Alma Ata (43.2°N, 76.9°E), and Wallops Island (37.9°N, 284.5°E), reveals that there is small longitude dependence in the overall seasonal behavior of dNmF2/dP (not shown). At those northern midlatitude stations dNmF2/dP is also higher at equinoxes and in winter and lower in months from June to August.

3.4. Contributions to the Solar Activity Variability of NmF2

[19] The ionosphere formation is described by the continuity equation

$$\frac{\partial N_i}{\partial t} = Q_i - \beta_i N_i + M.$$

Here M is the transport term, N_i the ion density, β_i the loss coefficient of ions, and Q_i the photoionization production rate of ions. Strictly speaking, the concentrations of electrons in the daytime *F* region should be determined by photoionization and chemical recombination, as well as transport processes [see *Rishbeth and Garriott*, 1969; *Ivanov-Kholodny and Mikhailov*, 1986].

[20] For simplicity, first ignoring the dynamic effect and assuming the ionosphere under a steady state, NmF2 is determined solely by photoionizations and recombinations at hmF2 during the daytime [*Rishbeth and Baron*, 1960]. In general, O^+ dominates in the ionospheric F2 layer [e.g., *Brekke*, 1997; *Lei et al.*, 2004]. The β_i depends on the concentrations of neutral N_2 and O_2 ($[N_2]$ and $[O_2]$): $\beta_i = k_1[N_2] + k_2[O_2]$, where k_1 and k_2 are the reaction rates of the two reactions: $O^+ + N_2 \xrightarrow{k1} NO^+ + N$; $O^+ + O_2 \xrightarrow{k2} O_2^+ O$. Both rate constants are temperature-dependent [*Hierl et al.*, 1997]. Under the chemical equilibrium and neglecting the molecular ions, which is reasonable when the daytime *F* layer is high [*Lei et al.*, 2004], the electron density

$$N_e = Q_i/\beta_i, \tag{3}$$

which depends on $[O]/[N_2]$ and the solar EUV fluxes. When the molecular ions dominate, β_i should be replaced with [*Brekke*, 1997, p. 218]

$$\beta_i' = \frac{\beta_i}{1 + \frac{k_1[N_2]}{\alpha_1 N_e} + \frac{k_2[O_2]}{\alpha_2 N_e}}.$$

Here α_1 and α_2 are the reaction rate constants of reactions: $NO^+ + e \xrightarrow{\alpha_1} N + O$; $O_2^+ + e \xrightarrow{\alpha_2} O + O$. Therefore

$$N_e = Q_i/\beta_i'. \tag{4}$$

[21] In the following calculations, parameters of neutral atmosphere are provided by the NRLMSIS00 model [*Picone et al.*, 2002], solar EUV fluxes are taken from the EUVAC model [*Richards et al.*, 1994a], and the absorption and ionization cross sections are also adopted from *Richards et al.* [1994a]. The reaction rate constants, k_1 and k_2, are adopted from *St.-Maurice and Torr* [1978] and *Pavlov et al.* [1999], and the rate constants α_1 and α_2 are adopted from *Brekke* [1997], respectively.

[22] Consider first the calculations at fixed height. The results for calculations made at fixed heights of 320 km are shown in Figure 6 and of 300 km in Figure 7 (top). As shown in Figure 6, with increasing solar activity, an atmospheric consequence is the significant increases in [O] and $[N_2]$ at the *F* layer heights. As a result, the enhanced solar activity causes a nonlinear decrease in $[O]/[N_2]$ at fixed heights, which is evidently different from that of NmF2. Two features can be easily detected from the results of the fixed height calculations. One is that Q_i/β_i' at a fixed height reproduces the observed saturation effect of NmF2 with P at high solar activity. It suggests that the neutral atmospheric consequences due to the solar activity variations should play an important role in producing the ionospheric saturation effect. The other is that the change rate of Q_i/β_i' with P is much less than the observed dNmF2/dP. This point is consistent with that of *Kane* [2003]. Therefore calculations at fixed height verify that the contributions from solar EUV as well as the neutral atmospheric consequences are inadequate for reproducing the observed solar activity changes of NmF2.

[23] Now we turn to the calculations at varied heights, because the height of the *F* layer peak is found to increase with solar activity variations [e.g., *Lei et al.*, 2005; *Pandey et al.*, 2003; *Richards*, 2001] in response to changes of ionization production, loss, and transport conditions. For example, the values of noon dhmF2/dP over Millstone Hill vary from 0.2 to 0.6 km per F107 unit (10^{-22} W m^{-2} Hz^{-1}) [*Lei et al.*, 2005]. Calculations are made at varied heights via the simple model:

$$h = h_0 + \frac{dh}{dP}(P - P_0). \tag{5}$$

Where h is the height in kilometer, dh/dP is the change rate of heights with P; and here we take $h_0 = 300$ km, $P_0 = 120 \times 10^{-22}$ W m^{-2} Hz^{-1}.

[24] Results at Hobart (42.9°S, 147.2°E) and Kokubunji (139.5°E, 35.7°N) are presented in Figure 7. As shown in Figure 7, the change rate of Q_i/β_i' with P, $d(Q_i/\beta_i')/dP$ increases with dh/dP. Thus the change rate of NmF2 with P should be contributed from the solar activity effect of hmF2. Compared with the fixed height case (see Figures 6 and 7 (top)), the observations are effectively reproduced by calculations with the varied height model (dh/dP = 0.35 km per 10^{-22} W m^{-2} Hz^{-1}). In essence, the role of dynamical effects played is partially implicitly taken into account with this simple varied-height model. Thus our calculations indicate that dynamical effects should have significant contributions to the solar activity variations of NmF2. Figure 7 (bottom) show the calculated $d(Q_i/\beta_i')/dP$ via the simple model (Equation (5)) with different values of dh/dP. The calculations via the simple model are capable of reproducing the observed solar activity change rate of NmF2 by adjusting the value of dh/dP.

[25] Further calculations at observed hmF2 are carried out at Wuhan in four seasons. Comparisons of observations and calculations are illustrated in Figure 8. The observed hmF2 at Wuhan from 1999 to 2004 are calculated from ionograms with a standard true height inversion program [*Reinisch and Huang*, 1983] inherent in the UMLCAR SAO-Explorer. Figure 8 illustrates the observed change rate of hmF2 with P

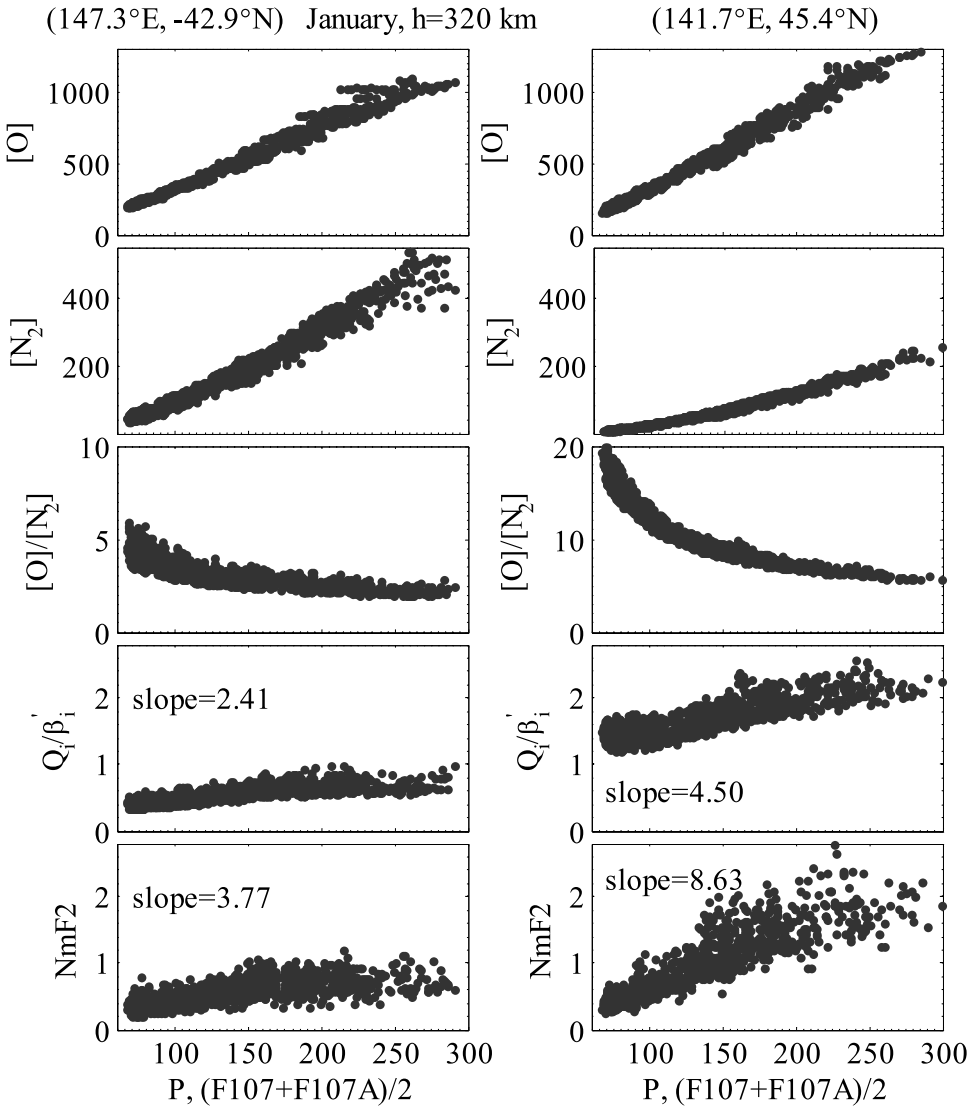

Figure 6. Scatterplots of the concentrations (in 10^{12} cm^{-3}) of neutral atom oxygen ([O]) and molecular nitrogen ([N_2]), the ratio of [O] to [N_2] ([O]/[N_2]), and calculated electron density (Q_i/β'_i in equation (3), in 10^6 electron cm^{-3}) at a fixed height of 320 km and observed NmF2 at (left) Hobart (42.9°S, 147.2°E) and (right) Wakkanai (45.4°N, 141.7°E) against the solar activity factor P in January, respectively. Neutral parameters are provided by the MSISE00 model. The slopes (in 10^3 cm^{-3} per 10^{-22} W m^{-2} Hz^{-1}) of the calculated electron density and observed NmF2 with P in the linear segment are labeled in the corresponding panels, respectively. P takes values of the previous day at the top three panels and on the current day at the bottom two panels.

varying from 0.43 km per 10^{-22} W m^{-2} Hz^{-1} in autumn to 0.66 km per 10^{-22} W m^{-2} Hz^{-1} in summer at Wuhan. Compared with the observations, the change rate of Q_i/β'_i at hmF2 is about the same in autumn, higher in spring and winter, and significantly higher in summer.

3.5. Dynamic Effect on the Solar Activity Variability of NmF2

[26] As shown above, the deviation of the observations from the calculations under the chemical equilibrium indicates that the dynamical effects may be important. The F2 peak is well known as being largely controlled by neutral winds and electric fields [*Buonsanto*, 1990; *Rishbeth*, 1993], which may also have solar activity variations [e.g., *Titheridge*, 1995; *Richards*, 2001; *Liu et al.*, 2004b]. Unfortunately, accurate knowledge of dynamical factors, especial the neutral winds, is still lacking for most locations [e.g., *Liu et al.*, 2004b]. Alternatively, the contribution of the dynamical effects to the solar activity variability of NmF2 can be roughly estimated by using the following equation given by *Ivanov-Kholodny and Mikhailov* [1986, p.44]

$$\lg \mathrm{NmF2} = 1.08 \lg[\mathrm{O}] - 0.65 \lg \beta + \lg \mathrm{I}/\mathrm{I}_{144} + 9 \times 10^{-3} \mathrm{W} - 5.8, \quad (6)$$

where I/I_{144} is the ratio between the total flux of the solar radiation and its value at the solar activity level F107 = 144

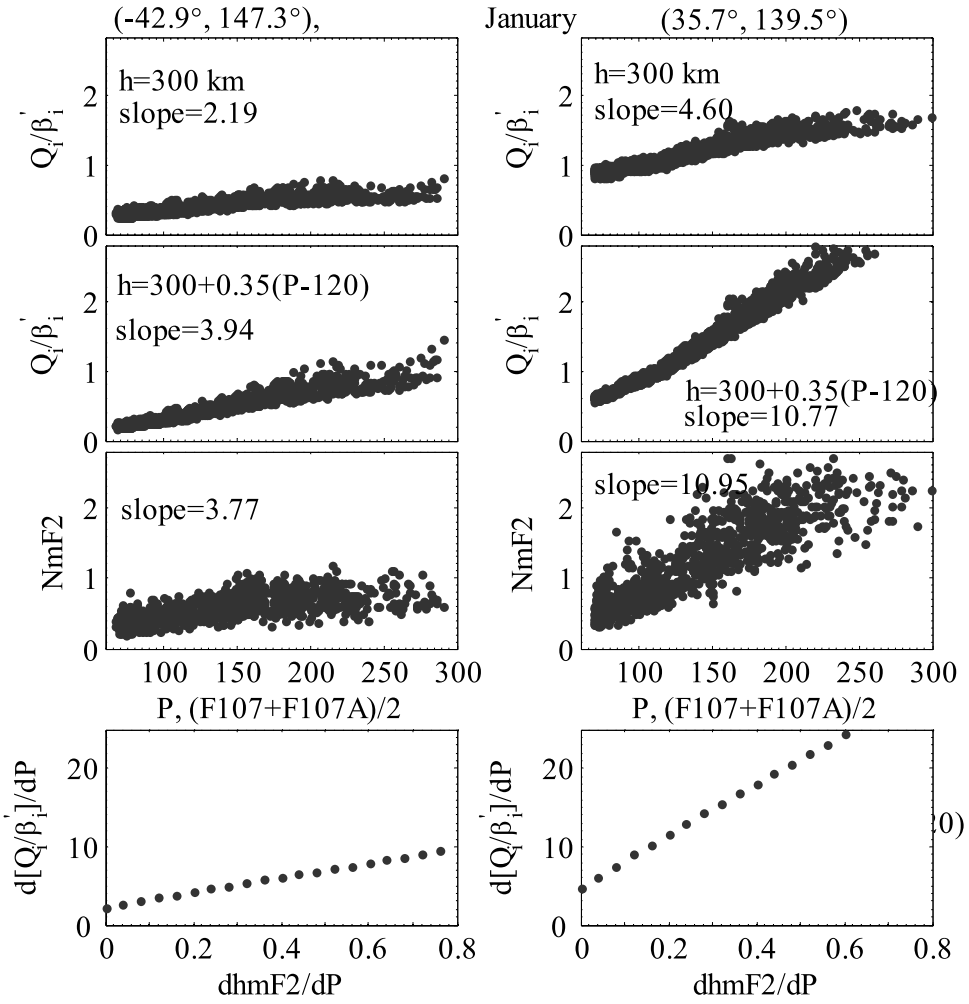

Figure 7. Scatterplots of the calculated electron density (Q_i/β'_i in equation (3), in 10^6 electron cm^{-3}) at a fixed height of 300 km, at height via a simple model h = 300 + 0.35(P-120) km, and observed NmF2 at (left) Hobart (42.9°S, 147.2°E) and (right) Kokubunji (35.7°N, 139.5°E) against the solar activity factor P in January, respectively. Neutral parameters are provided by the MSISE00 model. The slopes (in 10^3 cm^{-3} per 10^{-22} W m^{-2} Hz^{-1}) of the calculated electron density and observed NmF2 with P in the linear segment are labeled in the corresponding panels, respectively. P takes values of the current day. The slopes as a function of the change rate of ionospheric height with P (dh/dP, in km per 10^{-22} W m^{-2} Hz^{-1}) are plotted at the bottom panel.

(10^{-22} W m^{-2} Hz^{-1}); and W is the drift velocity (m s^{-1}), which represents the dynamic effects. Equation (6) is useful for making quantitative estimates of the contributions of individual atmospheric parameters at 300 km to the variation of the maximum electron concentration in the F2 layer [*Ivanov-Kholodny and Mikhailov*, 1986]. Note that measurements of the total solar flux are not available, thus the contributions from the solar flux are approximately evaluated from the two waveband SEM/SOHO EUV observations. The possible influence of this replacement was found insignificant by being evaluated with the EUVAC model.

[27] The values of lg[O], lgβ, and lg I/I_{144} over Wuhan at two solar activity levels are given in Table 3. Accordingly, Table 4 shows the possible contribution of the dynamic effect over Wuhan, which is estimated from the residual of the observed lg NmF2 and $1.08\lg[O] - 0.65\lg\beta + \lg I/I_{144} - 5.8$ as presented in Table 3. It is clearly seen from Table 4 that the solar variability of NmF2 over Wuhan is contributed from [O], β, and solar EUV, as well as the dynamic effects. The dynamic effect attenuates the solar activity variations of NmF2 over Wuhan, and its contributions are about 1/4 to 1/3, compared to other factors. It should be noted that at low and equatorial latitudes, the role of dynamic effects on the solar activity variations of NmF2 may be more important than that at middle latitudes. It may hint why the solar activity effect of electron density shown in Figure 5 is more sensitive at low latitudes than at midlatitudes.

4. Summary

[28] This paper investigated the solar activity dependence of NmF2 based on a series of daily solar EUV data from SEM/SOHO measurements and complete foF2 data now available at 20 ionosonde stations in the east Asia/Australia

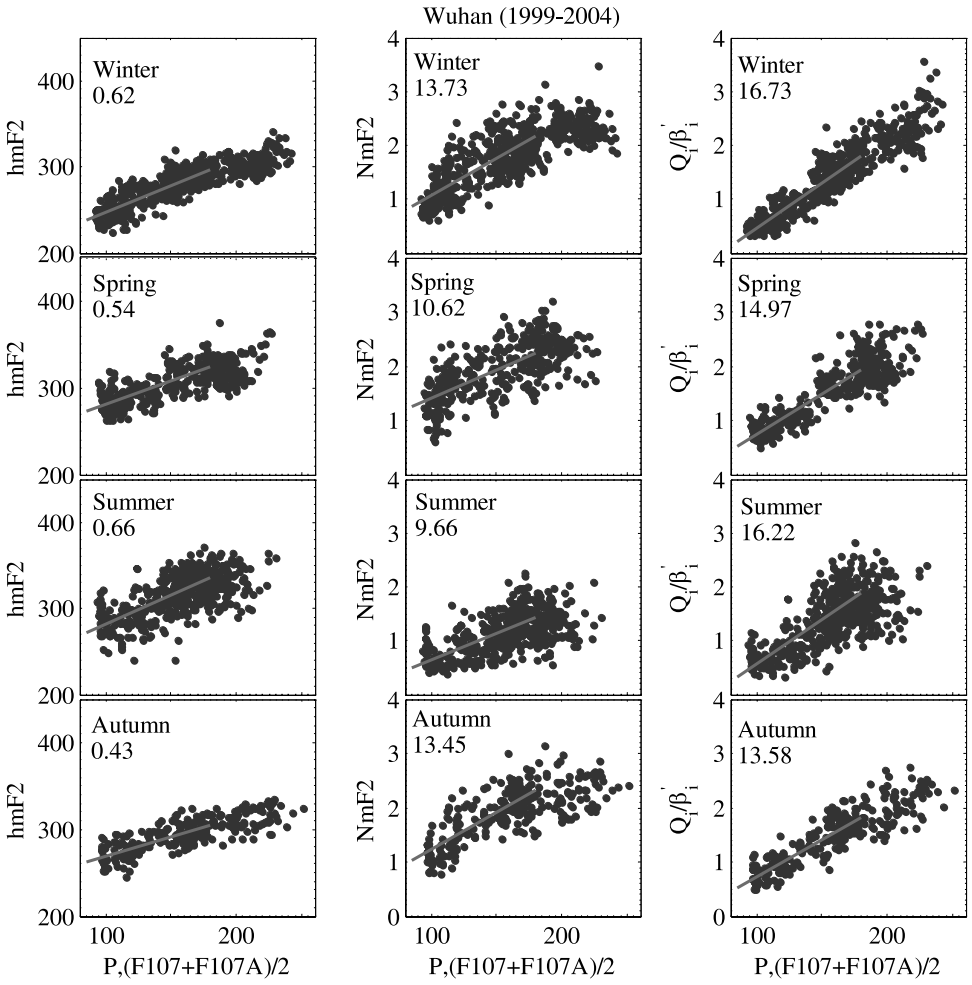

Figure 8. Mass plot of the daily noon (left) hmF2 (in km), (middle) NmF2, and (right) calculated electron density (Q_i/β'_i in equation (3), in 10^6 electron cm^{-3}) at hmF2 against P at Wuhan (114.4°E, 30.6°N) during 1999–2004 in four seasons. The slopes (dhmF2/dP in km per 10^{-22} W m^{-2} Hz^{-1}, dNmF2/dP and $d(Q_i/\beta'_i)/dP$ in 10^3 electron cm^{-3} per 10^{-22} W m^{-2} Hz^{-1}) are also labeled, respectively.

sector. The SEM/SOHO EUV observations and NmF2 data provide a good opportunity to study the solar activity variability in the ionosphere. The conclusions can be drawn as follows:

[29] 1. The SEM/SOHO EUV observations show a nonlinear relationship between solar EUV and F107, and the solar activity factor P = (F107 + F107A)/2 can better represent the intensities of SEM/SOHO EUV than F107.

[30] 2. At high values of the solar EUV flux, a saturation effect is visible in the observed NmF2, which suggests that the saturation effect in NmF2 cannot be solely attributed to the nonlinear representation of EUV by F107. Therefore the saturation effect should be contributed from the atmospheric consequences, as well as the ionosphere itself via the dynamical effects.

[31] 3. Seasonal and latitudinal dependences are found in the solar activity variation of NmF2 at 20 ionosonde stations in the east Asia/Australian sector. The slope of NmF2 with P in the linear segment further shows similar annual variations as the background electron densities.

Table 3. Contributions of Individual Parameters to the Observed NmF2 Over Wuhan According to Equation (6)

	Winter		Summer		Spring		Autumn	
Parameter	P = 90	P = 170	P = 90	P = 170	P = 90	P = 170	P = 90	P = 170
lg $I/I_{144\ (0.1-50\ nm)}$, 10^{10} photons cm^{-2} s^{-1}	−0.235	0.079	−0.226	0.077	−0.207	0.073	−0.235	0.079
lg $I/I_{144\ (26-34\ nm)}$, 10^{10} photons cm^{-2} s^{-1}	−0.223	0.077	−0.213	0.074	−0.193	0.069	−0.220	0.076
lg[O], cm^{-3}	8.669	9.006	8.605	8.947	8.725	9.045	8.711	9.075
lgβ, s^{-1}	−4.197	−3.836	−4.051	−3.669	−4.044	−3.659	−4.134	−3.720
lg NmF2, cm^{-3}	5.975	6.314	5.776	6.112	6.102	6.351	6.036	6.350
Residual $_{0.1-50\ nm}$, cm^{-3}	−0.081	−0.185	−0.125	−0.213	0.057	−0.069	−0.024	−0.148
Residual $_{26-34\ nm}$, cm^{-3}	−0.093	−0.183	−0.138	−0.209	0.043	−0.065	−0.039	−0.145

Table 4. Contributions of Individual Parameters to the Observed Solar Activity Variations of NmF2 Over Wuhan According to Equation (6)

Term	Winter	Summer	Spring	Autumn
Δlg $I_{(0.1-50\ nm)}$, 10^{10} photons cm^{-2} s^{-1}	0.314	0.303	0.280	0.314
Δlg $I_{(26-34\ nm)}$, 10^{10} photons cm^{-2} s^{-1}	0.300	0.287	0.262	0.296
Δlg[O], cm^{-3}	0.337	0.342	0.320	0.364
Δlgβ, s^{-1}	0.361	0.382	0.385	0.414
Δlg NmF2, cm^{-3}	0.339	0.336	0.249	0.314
Residual $_{0.1-50\ nm}$, cm^{-3}	−0.104	−0.088	−0.126	−0.124
Residual $_{26-34\ nm}$, cm^{-3}	−0.090	−0.071	−0.108	−0.106

[32] 4. Roles of ionospheric photochemistry and of the neutral upper atmosphere and the influence of dynamics (via a simple model of the solar activity effect of hmF2) are estimated. Calculations at fixed height can well reproduce the observed saturation effect, but the change rate of the calculated electron density with P is inadequate reproduced. The observed dNmF2/dP can be roughly reproduced by taking the solar activity effect of ionospheric height into account. The rough estimations may reproduce the main features of the solar activity variations of NmF2.

[33] Besides solar EUV changes, the atmospheric consequences and the solar activity effects of hmF2, as well as the dynamical effects, also definitively contribute to the solar activity changes in NmF2. Although calculations via the simple model allowed us to partially reproduce the main observed features, the extent of contributions from dynamic effects (from neutral winds and electric fields) to the solar activity variations of NmF2 needs further investigation.

[34] **Acknowledgments.** The authors thank two referees and Clia Goodwin for their valuable suggestions for improving the presentation of the paper. The Ap and F107 indices are downloaded from the SPIDR Web site http:/spidr.ngdc.noaa.gov/. Ionospheric data are provided from WDC for Ionosphere, Tokyo, National Institute of Information and Communications Technology, WDC for Solar-Terrestrial Science which is operated by IPS Radio and Space Services of Australia, and from SPIDR. The SEM/SOHO EUV data are downloaded from the Web site http://www.usc.edu/dept/space_science/semdatafolder/long/. The CELIAS/SEM experiment on the Solar Heliospheric Observatory (SOHO) spacecraft (SOHO is a joint European Space Agency, U.S. National Aeronautics and Space Administration mission). NSO/Kitt Peak data used here are produced cooperatively by NSF/NOAO, NASA/GSFC, and NOAA/SEC. The NOAA Mg II daily index version 9.1 is prepared by the U.S. Department of Commerce, NOAA, Space Environment Center. This research was supported by National Natural Science Foundation of China (40574071), the KIP Pilot Project (kzcx3-sw-144) of Chinese Academy of Sciences, and National Important Basic Research Project (2006CB806306).

[35] Amitava Bhattacharjee thanks Jiuhou Lei and J. Michael Picone for their assistance in evaluating this paper.

References

Adler, N. O., A. G. Elias, and J. R. Manzano (1997), Solar cycle length variation: Its relation with ionospheric parameters, *J. Atmos. Sol. Terr. Phys.*, *59*(2), 159–162.

Balan, N., G. J. Bailey, B. Jenkins, P. B. Rao, and R. J. Moffett (1994), Variations of ionospheric ionization and related solar fluxes during an intense solar cycle, *J. Geophys. Res.*, *99*, 2243–2253.

Balan, N., G. J. Bailey, and Y. Z. Su (1996), Variations of the ionosphere and related solar fluxes during solar cycles 21 and 22, *Adv. Space Res.*, *18*(3), 11–14.

Bilitza, D. (2000), The importance of EUV indices for the International Reference Ionosphere, *Phys. Chem. Earth, Part C*, *25*(5–6), 515–521.

Brekke, A. (1997). *Physics of the Upper Polar Atmosphere*, 485 pp., John Wiley, Hoboken, N. J.

Buonsanto, M. J. (1990), Observed and calculated F2 peak heights and derived meridional winds at mid-latitudes over a full solar cycle, *J. Atmos. Terr. Phys.*, *52*, 223–240.

Floyd, L., J. Newmark, J. Cook, L. Herring, and D. McMullin (2005), Solar EUV and UV spectral irradiances and solar indices, *J. Atmos. Sol. Terr. Phys.*, *67*, 3–15.

Forbes, J. M., S. E. Palo, and X. Zhang (2000), Variability of the ionosphere, *J. Atmos. Sol. Terr. Phys.*, *62*, 685–693.

Harvey, J. W. (1984), Helium 10830 Å irradiance: 1975–1983, in *Solar Irradiance Variations on Active Region Time Scales*, *NASA Conf. Publ., 2310,* 197–221.

Hierl, P. M., I. Dotan, J. V. Seeley, J. M. Van Doren, R. A. Morris, and A. A. Viggiano (1997), Rate constants for the reactions of O+ with N2 and O2 as a function of temperature (300–1800K), *J. Chem. Phys.*, *106*, 3540–3544.

Hinteregger, H. E., K. Fukui, and B. R. Gilson (1981), Observational, reference and model data on solar EUV, from measurements on AE-E, *Geophys. Res. Lett.*, *8*, 1147.

Huang, Y., and K. Cheng (1995), Solar cycle variation of the total electron content around equatorial anomaly crest region in east Asia, *J. Atmos. Terr. Phys.*, *57*, 1503–1511.

Ivanov-Kholodny, G. S., and A. V. Mikhailov (1986), *The Prediction of Ionospheric Conditions*, 167 pp., Springer, New York.

Judge, D., et al. (1998), First solar EUV irradiances obtained from SOHO by the SEM, *Sol. Phys.*, *177*, 161–173.

Kane, R. P. (1992), Sunspots, solar radio noise, solar EUV and ionospheric foF2, *J. Atmos. Terr. Phys.*, *54*, 463–466.

Kane, R. P. (2003), Solar EUV and ionospheric parameters: A brief assessment, *Adv. Space Res.*, *32*(9), 1713–1718.

Kawamura, S., N. Balan, Y. Otsuka, and S. Fukao (2002), Annual and semiannual variations of the midlatitude ionosphere under low solar activity, *J. Geophys. Res.*, *107*(A8), 1166, doi:10.1029/2001JA000267.

Kouris, S. S., P. A. Bradley, and P. Dominici (1998), Solar-cycle variation of the daily foF2 and M (3000)F2, *Ann. Geophys.*, *16*, 1039–1042.

Kuznetsov, V. V., V. V. Plotkin, G. V. Nesterova, and I. I. Nesterova (1998), Universal variation of the F2-layer critical frequency and solar activity, *Earth Planets Space*, *50*, 57–61.

Lean, J. L., O. R. White, W. C. Livingston, and J. M. Picone (2001), Variability of a composite chromospheric irradiance index during the 11-year activity cycle and over longer time periods, *J. Geophys. Res.*, *106*, 10,645–10,658.

Lei, J., L. Liu, W. Wan, and S.-R. Zhang (2004), Model results for the ionospheric lower transition height over mid-latitude, *Ann. Geophys.*, *22*, 2037–2045.

Lei, J., L. Liu, W. Wan, and S.-R. Zhang (2005), Variations of electron density based on long-term incoherent scatter radar and ionosonde measurements over Millstone Hill, *Radio Sci.*, *40*, RS2008, doi:10.1029/2004RS003106.

Liu, J. Y., Y. I. Chen, and J. S. Lin (2003), Statistical investigation of the saturation effect in the ionospheric foF2 versus sunspot, solar radio noise, and solar EUV radiation, *J. Geophys. Res.*, *108*(A2), 1067, doi:10.1029/2001JA007543.

Liu, L., W. Wan, and B. Ning (2004a), Statistical modeling of ionospheric foF2 over Wuhan, *Radio Sci.*, *39*, RS2013, doi:10.1029/2003RS003005.

Liu, L., X. Luan, W. Wan, J. Lei, and B. Ning (2004b), Solar activity variations of equivalent winds derived from global ionosonde data, *J. Geophys. Res.*, *109*, A12305, doi:10.1029/2004JA010574.

Liu, L., W. Wan, and B. Ning (2006), A study of the ionogram derived effective scale height around the ionospheric hmF2, *Ann. Geophys.*, *24*, 851–860.

Mikhailov, A. V., and V. V. Mikhailov (1995a), Solar cycle variations of annual mean noon foF2, *Adv. Space Res.*, *15*(2), 79–82.

Mikhailov, A. V., and V. V. Mikhailov (1995b), A new ionospheric index MF2, *Adv. Space Res.*, *15*(2), 93–97.

Mikhailov, A. V., and K. Schlegel (2000), A self-consistent estimate of $O^+ + N_2$–rate coefficient and total EUV solar flux with $\lambda < 1050$Å using EISCAT observations, *Ann. Geophys.*, *18*, 1164–1171.

Pancheva, D., and P. Mukhtarov (1998), A single-station spectral model of the monthly median foF2 and M (3000)F2, *Stud. Geophys. Geod.*, *42*, 183–196.

Pandey, V. K., N. K. Sethi, and K. K. Mahajan (2003), Dependence of F2-peak height on solar activity: A study with incoherent scatter measurements, *Adv. Space Res.*, *31*(3), 543–548.

Pavlov, A. V., M. J. Buonsanto, A. C. Schlesier, and P. G. Richards (1999), Comparison of models and data at Millstone Hill during the 5–11 June 1991 storm, *J. Atmos. Sol. Terr. Phys.*, *61*, 263–279.

Picone, J. M., A. E. Hedin, D. P. Drob, and A. C. Aikin (2002), NRLMSISE-00 empirical model of the atmosphere: Statistical comparisons and scientific issues, *J. Geophys. Res.*, *107*(A12), 1468, doi:10.1029/2002JA009430.

Rao, M. S. J. G., and R. S. Rao (1969), The hysteresis variation in F2-layer parameters, *J. Atmos. Terr. Phys.*, *31*, 1119–1125.

Rastogi, R. G., and R. P. Sharma (1971), Ionospheric electron content at Ahmedabad (near the crest of equatorial anomaly) by using beacon satellite transmissions during half a solar cycle, *Planet. Space Sci.*, *19*(11), 1505–1517.

Reinisch, B. W., and X. Huang (1983), Automatic calculation of electron density profiles from digital ionograms: 3. Processing of bottomside ionograms, *Radio Sci.*, *18*(3), 477–492.

Richards, P. G. (2001), Seasonal and solar cycle variations of the ionospheric peak electron density: Comparison of measurement and models, *J. Geophys. Res.*, *106*, 12,803–12,819.

Richards, P. G., J. A. Fennelly, and D. G. Torr (1994a), EUVAC: A solar EUV flux model for aeronomic calculations, *J. Geophys. Res.*, *99*, 8981–8992.

Richards, P. G., D. G. Torr, B. W. Reinisch, R. R. Gamache, and P. J. Wilkinson (1994b), F2 peak electron density at Millstone Hill and Hobart: Comparison of theory and measurement at solar maximum, *J. Geophys. Res.*, *99*, 15,005–15,016.

Rishbeth, H. (1993), Day-to-day ionospheric variations in a period of high solar activity, *J. Atmos. Terr. Phys.*, *55*, 165–171.

Rishbeth, H., and D. W. Baron (1960), Equilibrium electron distributions in the ionospheric F2–layer, *J. Atmos. Terr. Phys.*, *18*, 234–252.

Rishbeth, H., and O. K. Garriott (1969), *Introduction to Ionospheric Physics*, 331 pp., Elsevier, New York.

Rishbeth, H., I. C. F. Müller-Wodarg, L. Zou, T. J. Fuller-Rowell, G. H. Millward, R. J. Moffett, D. W. Idenden, and A. D. Aylward (2000), Annual and semiannual variations in the ionospheric F2–layer: II. Physical discussion, *Ann. Geophys.*, *18*, 945–956.

Rishbeth, H., and C. S. G. K. Setty (1961), The F layer at sunrise, *J. Atmos. Terr. Phys.*, *10*, 263–276.

Sethi, N. K., M. K. Goel, and K. K. Mahajan (2002), Solar cycle variations of fo F2 from IGY to 1990, *Ann. Geophys.*, *20*, 1677–1685.

Sojka, J. J., C. Smithtro, and R. W. Schunk (2006), Recent developments in ionosphere– thermosphere modeling with an emphasis on solar-variability, *Adv. Space Res.*, *37*(2), 369–379.

St.-Maurice, J.-P., and D. G. Torr (1978), Nonthermal rate coefficients in the ionosphere: The reactions of O^+ with N_2, O_2, and NO, *J. Geophys. Res.*, *83*, 969–977.

Su, Y. Z., G. J. Bailey, and S. Fukao (1999), Altitude dependences in the solar activity variations of the ionospheric electron density, *J. Geophys. Res.*, *104*, 14,879–14,891.

Titheridge, J. E. (1995), Winds in the ionosphere-a review, *J. Atmos. Terr. Phys.*, *57*, 1681–1714.

Tobiska, W. K., T. Woods, F. Eparvier, R. Viereck, L. Floyd, D. Bouwer, G. Rottman, and O. R. White (2000), The Solar2000 empirical solar irradiance model and forecast toll, *J. Atmos. Sol. Terr. Phys.*, *62*, 1233–1250.

Triskova, L., and J. Chum (1996), Hysteresis in dependence of foF2 on solar indices, *Adv. Space Res.*, *18*(6), 145–148.

Viereck, R. A., and L. C. Puga (1999), The NOAA Mg II core-to-wing solar index: Construction of a 20-year time series of chromospheric variability from multiple satellites, *J. Geophys. Res.*, *104*, 9995–10,005.

Viereck, R. A., L. E. Floyd, P. C. Crane, T. N. Woods, B. G. Knapp, G. Rottman, M. Weber, L. C. Puga, and M. T. DeLand (2004), A composite Mg II index spanning from 1978 to 2003, *Space Weather*, *2*, S10005, doi:10.1029/2004SW000084.

Woods, T. N., and G. J. Rottman (1997), Solar Lyman alpha irradiance measurements during two solar cycles, *J. Geophys. Res.*, *102*, 8769–8779.

Yu, T., W. Wan, L. Liu, and B. Zhao (2004), Global scale annual and semiannual variations of daytime NmF2 in the high solar activity years, *J. Atmos. Sol. Terr. Phys.*, *66*, 1691–1701.

V. I. Kurkin and O. M. Pirog, Institute of Solar-Terrestrial Physics, Russian Academy of Sciences, Irkutsk 664033, Russia.

L. Liu, B. Ning, and W. Wan, Institute of Geology and Geophysics, Chinese Academy of Sciences, Beijing 100029, China. (liul@mail.igcas.ac.cn)